RSC Advances

ROYAL SOCIETY OF CHEMISTRY

www.rsc.org/advances

Recent progress in highly efficient Ag-based visible-light photocatalysts

Gaiping Li,[a] Yuexiang Wang,[b] and Lanqun Mao[*,b]

[a] Department of Chemistry, Zhengzhou University, Zhengzhou, 450001, China.

[b] Beijing National Laboratory for Molecular Sciences, Key Laboratory of Analytical Chemistry for Living Biosystems, Institute of Chemistry, the Chinese Academy of Sciences (CAS), Beijing, 100190, China.

[*] To whom correspondence should be addressed: Email: lqmao@iccas.ac.cn

Abstract

As one of the most promising and efficient approaches for remediating the deterioration of natural environments, semiconductor-based photocatalysis has received much attention. To date, numerous efforts have been focused on searching for novel materials for highly efficient photocatalysis under visible light or sunlight irradiation. Among them, Ag-based compounds are emerging as a more promising candidate due to their excellent visible light-responsive photoelectrochemical properties. This review summarizes the recent progress in the design and fabrication of Ag-compound based semiconductor photocatalysts and their applications in photocatalytic decomposition of organic molecules. We will start with discussion of the mechanisms of related photocatalytic reactions. Then, we will highlight some progresses in Ag-based micro- or nano-structured materials fabrication with enhanced photocatalytic performance. These novel and highly efficient photocatalysts mainly include Ag_2O, Ag_2S, AgX (X=Cl, Br, I), Ag_2CO_3 and Ag_3PO_4. We expect the present tutorial review will provide insights to direct the future visible-light photocatalyst design.

1. Introduction

Over the past decades, ever increasing environmental pollution and fossil energy shortages have substantially attracted the global attention. In order to solve these problems and realize the sustainable development of human society, it is urgent to develop available technologies for remediating the deterioration of natural environments[1-2] and generating the alternative clean energy.[3-5] As a potential solution, semiconductor-based photocatalysis have attracted tremendous interests, especially since 1972 when Fujishima and Honda discovered that water molecule could split into H_2 and O_2 on titania (TiO_2) electrode under UV light irradiation.[6] In this sense, photocatalysis can be regarded as a light-driven reaction, which is an environment-friendly and efficient approach for dealing with the environmental pollution[7-8] and producing hydrogen energy.[9]

The unique electronic structure of semiconductor materials, consisting of a filled valence band (VB) and an empty conduction band (CB), plays a crucial role in photoelectrochemical processes mentioned above. By absorbing photon energy equal to or higher than its band gap energy, the electrons in the VB are promoted to the CB, leaving an equal number of vacant sites (holes) in the VB. The photo-generated electrons and holes migrate to the surface of semiconductor and react with the adsorbed electron acceptors and electron donors, respectively. Hence these relevant reduction and oxidation reactions made up the fundamental mechanisms of semiconductor photochemistry. Theoretically, the semiconductor materials that meet the requirements mentioned above could be potentially used as photocatalysts for photoelectrochemical reactions. So far, more than 190 different semiconductors have been demonstrated as suitable photocatalysts for photoelectrochemical applications.[9] Among them, TiO_2 still remains the most widely studied photocatalyst. However,

TiO_2 only responds to high-energy UV light owing to its wide band gap. As known, one of the most fascinating aspects of photocatalysis technology is rooted in the possibility of employing sunlight, the most reliable, abundant and 'green' energy source under mild conditions. But UV light only accounts for less than 5% of the solar energy reached to the earth, which limits the efficient utilization of solar energy and thus the real-world applications of TiO_2. Since the major component of the solar radiation is visible light, developing the efficient visible-light responsive photocatalysts has thus become one of the most important objectives.[10] However, such a pursuit remains to be a great challenge.

There are a variety of strategies that can be used to improve the usage of solar energy to make the photocatalysis technology cost effective. Extensive researches have been focused on improving the photocatalytic activity of TiO_2 through, for example, doping with foreign elements[11-13] to modulate the energy band gap, combining with noble metals[14] or other semiconductors,[15] and adding quantum dots[16-17] or dyes[18] for light sensitization. Although these strategies could to some extent improve the visible-light photocatalytic performance of TiO_2, the activities and efficiencies in the utilization of solar irradiation over these state-of-art TiO_2-based semiconductor materials are still not satisfactory from the practical application point of view. Thereby, exploration and creation of new semiconductor materials that can be used as highly efficient visible-light photocatalysts are highly desirable.

Very recently, a series of Ag-based compounds including Ag_2O,[19] Ag_2S,[20] AgX (X=Cl, Br, I),[21-23] Ag_2CO_3[24] and Ag_3PO_4[25] have been demonstrated to possess excellent photoelectrochemical activities under the illumination of visible light or sunlight. Especially, an extremely high apparent quantum yields of nearly 90% under visible light (λ = 420 nm) has been achieved with Ag_3PO_4 as the photocatalyst for the

evolution of O_2 in water photolysis.[25] Since many important results have been reported on the Ag-based semiconductor photocatalysts over the past a few years, it seems a great opportunity to summarize the recent cutting-edge development in visible-light photocatalysts. In this review article, we will focus on the recent achievements in the Ag compounds-based photocatalysts from the standpoint of photoelectrochemistry, highlighting the recent progresses in the fabrication, modification and applications of this kind of photocatalysts. In addition, the mechanisms of the related photocatalytic reactions will also be discussed.

2. Principles of Ag-based photocatalysis

In essence, photocatalysis is to initiate or accelerate specific reduction and oxidation reactions with the assistance of irradiated semiconductors. Ag-based compounds are a kind of photosensitive materials, which tend to decompose easily under illumination. For example, a silver halide particle can generate an electron and a hole upon absorbing a photon, and then the photo-generated electron reduces an Ag^+ to Ag^0 atom. With absorbing more photons, a cluster of silver atoms is deposited on the silver halide particle. Due to their instability under sunlight, Ag-based compounds, especially silver halides, are extensively used in photography, but are seldom used as photocatalysts until recently.

In 1999, Kakuta and coworkers reported $AgBr/SiO_2$ photocatalyzed H_2 production from CH_3OH/H_2O solution under UV irradiation.[26] They observed that Ag^0 species were only generated at the initial stage of the reaction, and AgBr did not deconstruct further under successive UV irradiation. As suggested, the metallic Ag could trap photo-induced electrons, which inhibited further reduction of Ag^+ and promoted charge separation in contact with a photoexcited semiconductor. Thus, the resulting

Ag/Ag salts composites are stable under irradiation because the photo-induced electrons enrich in the Ag nanoparticles (NPs) on the surface rather than being transferred to the Ag salts. The self-stabilization mechanism has been highlighted by many researches, namely, the metal Ag arising from the partial photodecomposition of Ag salts by illumination, enhancing the structure stability of Ag salts. In general, this mechanism holds true for almost all the Ag-compound-based photocatalysts including Ag_2O, AgX (X=Cl, Br, I), Ag_2CO_3 and Ag_3PO_4.

In addition to the stability, Ag-compound-based photocatalysts bear high photocatalytic efficiency. As well known that, noble metal nanoparticles (NPs), such as Au NPs and Ag NPs, show efficient plasmon resonance in the visible region because of the localized surface plasmon resonance (LSPR) effect,[27-28] which leads to the strong absorption of the sunlight. The LSPR effect of noble metal NPs have been utilized to improve the performance of semiconductor photocatalysts and to develop new plasmonic photocatalysts.[29-33] Additionally, the excellent conductivity of Ag NPs can promote the electron transfer so as to suppress electron-hole recombination and can thus enhance the interfacial charge transfer. Therefore, Ag NPs supported on silver salts particles might be expected to be highly efficient and stable visible-light photocatalysts.[21] The underlying mechanisms will be discussed below. Studies on Ag-compound photocatalytic mechanism under visible light irradiation have been put forward recently. In the case of wide band gap materials which visible light energy could not suffice, such as AgCl (direct band gap of 5.6 eV and indirect band gap of 3.25 eV), Ag NPs facilitates the photocatalysis and a novel mechanism of Ag plasmonic photocatalysis was proposed.[21] It has been suggested that a photon is absorbed by an Ag NP, leading to the separation of an electron and a hole due to the dipolar character of the surface plasmon state of Ag NPs. The AgCl particle is

negatively charged since its surface is mostly terminated by Cl^- ions. Consequently, free electrons in the Ag NPs are polarized by the AgCl core and, as a result, the regions of negative and positive charges in the Ag NPs are far from and close to the Ag/AgCl interface, respectively. In other words, the electron-hole separation and interfacial charge transfer could be efficiently facilitated by the synergetic effect between the dipolar characters of the surface plasmon state of Ag NPs and the polarization field provided by the AgCl core. As a result, the electrons are enriched on the surface of Ag NPs and are far away from the AgCl core, eliminating the reduction of AgCl and eventually leading to a high stability of the composite materials. Meanwhile, holes diffuse into the AgCl core and promote the oxidation of Cl^- ions to Cl^0 atoms that are very reactive for oxidizing organic molecules. The electrons are then trapped by O_2 dissolved in the solution to form the reactive oxygen species that can also chemically oxidize the organic compounds in the photocatalytic process. All these factors contribute to a high catalytic efficiency of AgCl photocatalyst.

For the narrow band gap materials such as Ag_2O (1.2 eV), Ag_2CO_3 (2.30 eV), AgBr (2.69 eV), and Ag_3PO_4 (direct bandgap of 2.43 eV and indirect bandgap of 2.36 eV), the conventional photocatalytic process occurs due to the fact that these semiconductor materials can be directly excited under visible light illumination. Taking Ag_2O as an example, when Ag_2O photocatalyst is irradiated with visible light, a number of electron-hole pairs are generated; given that the more positive potential of Ag^+/Ag (0.7991 V, *vs*. SHE) compared with O_2/HO_2 (-0.046 V, *vs*. SHE), the photo-induced electrons in the CB preferably combine with Ag^+ ions to form Ag NPs in the early stage of the reaction; the photo-induced electrons enriched on the as-formed Ag NPs are expected to be trapped by O_2 dissolved in the solution to form the reactive oxygen species, and the photo-induced holes in the VB oxidize the

organic substances directly (see Fig. 1).[19] It has been expected that, the novel Ag plasmonic photocatalysis mechanism might coexist in these photocatalytic systems.

3. Synthesis and modification of Ag-compound based photocatalysts

3.1 Ag compounds-based photocatalysts

In order to improve the utilization of solar energy, much effort has been devoted to developing new visible-light-sensitive photocatalysts with highly efficient photoelectrochemical performance. Recently, a series of Ag compounds have been studied and demonstrated to be novel photocatalysts with excellent performance under visible light irradiation.

3.1.1 Ag/Ag oxosalts photocatalysts

Wang et al. synthesized Ag_2O powder via a typical precipitation reaction of silver nitrate and sodium hydroxide at room temperature.[19] Under fluorescent light irradiation, the Ag_2O sample exhibited a higher photocatalytic activity toward the degradation of methyl orange (MO) than the typical visible-light photocatalyst N-TiO_2. Further investigation revealed that Ag_2O photocatalyst could also effectively decolorize rhodamine B (RhB) in an aqueous solution under fluorescent light irradiation and decompose a colorless phenol solution under visible light irradiation, demonstrating that Ag_2O material could be used as a new kind of potential visible-light-responsive photocatalyst.

On the other hand, theoretical studies of electronic band structure suggest that it is an effective strategy to change the crystal structure and thereby adjust the bandgap by incorporating of p-block element into a simple narrow bandgap oxide.[25] Ag_2O is a semiconductor with a narrow band gap of 1.3 eV and thus adding p-block elements into Ag_2O may pave a new approach to the development of new visible-light-sensitive

photocatalysts. As expected, yellow green Ag_2CO_3 powder with a larger band gap of 2.30 eV was prepared by a simple precipitation reaction between $NaHCO_3$ and $AgNO_3$.[24] The as-formed Ag_2CO_3 powder showed a high catalytic activity towards the decomposition of many kinds of dyes including RhB, MO and methylene blue (MB). However, the photocatalytic activity decreased gradually in the cyclic experiments owing to the decomposition of Ag_2CO_3 itself under light irradiation. A possible approach to inhibit the photocorrosion of Ag_2CO_3 was proposed by Dai and coworkers.[34] They found that the enhanced photoactivity of Ag_2CO_3 could be achieved with the presence of $AgNO_3$. In this photocatalytic system, $AgNO_3$ acted as a scavenger for electrons to effectively separate the photo-generated electron-hole pairs owing to the lower potential of $Ag/AgNO_3$ than that of Ag/Ag_2CO_3, and thus the photocorrosion of Ag_2CO_3 was inhibited.

The other successful example was adopting non-metal P element to tune the low-lying CB of Ag_2O. The golden colored Ag_3PO_4 powder prepared by a simple ion-change method could efficiently absorb solar energy at a wavelength shorter than 530 nm (Fig. 2A and 2C).[25] Under visible light illumination, Ag_3PO_4 powder displays extremely high photooxidative abilities for the evolution of O_2 from water (Fig. 2B) and for the decomposition of MB dye (Fig. 2D). In particular, the achieved high apparent quantum yields at wavelength in the region from 400 to 480 nm (Fig. 2C) were obviously higher than the values reported so far. A comparative study of the electronic structures of Ag_3PO_4 and Ag_2O revealed that CB was constructed mainly through Ag *s* states in Ag_3PO_4 and Ag *d* states in Ag_2O.[35] The excellent photocatalytic performance of Ag_3PO_4 was attributed partly to the highly dispersive Ag *s*-Ag *s* bands without localized *d* states at CB, realizing a small effective mass of the electron and thus eliminating the carrier recombination.[35-36]

Furthermore, the photocatalytic activities of various silver oxosalts $Ag_x(XO_y)_z$, such as Ag_3AsO_4, Ag_2CO_3, Ag_3PO_4, Ag_2SO_4, and Ag_2SeO_4, have also been systematically investigated.[37] The results revealed that the optical band gaps of silver oxosalts increased linearly with increasing the charge-to-size (Z/r) ratio of the central atom X, whereas the surface charge of silver oxosalts decreased with increasing the Z/r ratio. Except for Ag_2SO_4, all the silver oxosalts were fairly active under visible light irradiation, and the overall photocatalytic efficiency decreased in the order of Ag_3PO_4 > Ag_3AsO_4 > Ag_2CO_3 > Ag_2SeO_4 > Ag_2SO_4, which roughly matched with the relative orders of their band gaps, suggesting the Z/r ratio of central atom provides a facile and effective measure for predicting the optical band gap and photocatalytic performance of silver oxosalts.

3.1.2 Ag/AgX photocatalysts

In the Ag-compound based photocatalytic systems, silver halides, such as AgCl, AgBr and AgI are the other kind of extensively studied photocatalysts. Considering that silver halides can spontaneously decompose to metallic Ag on light irradiation, and the resulting metallic Ag plays a key role in stabilizing the silver halides, the AgX particles with Ag NPs modified on their surface (referred to as Ag@AgX particles for convenience) might be expected to be stable photocatalysts.[21] This expectation has been demonstrated by recent reports on the synthesis of Ag@AgX particles. For example, Wang and coworkers produced the Ag@AgCl particles by two steps: firstly treating Ag_2MoO_4 with HCl to form AgCl particles and then reducing some Ag^+ ions via photo-reduction method.[21] In the photo-reduction process, Ag^+ ions were used for scavengers of photo-generated electrons to form Ag NPs with diameters of 20-150 nm on the surface of AgCl particles. In addition, a chemical reduction method by using sodium borohydride ($NaBH_4$) as the reduction agent was also employed to prepare

Ag@AgCl nanocubes.[38] Later, An et al. developed an efficient one-pot approach for the synthesis of hybrid nanoparticles composed of AgCl cores coated with Ag nanograins, involving a precipitation reaction followed by polyol reduction at a temperature of 160℃.[22] Another one-pot hydrothermal method with the help of ionic liquid 1-octyl-3-methylimidazolium chloride ([Omim]Cl), which acted as a precursor and a reducing reagent, was also reported.[39] All the obtained Ag@AgCl particles showed a strong adsorption in the visible region because of the plasmon resonance of Ag NPs, and exhibited high activity and durability towards degradation of the dye molecules such as MO and MB under visible light or sunlight irradiation.

As an analogous photocatalyst, Ag@AgBr prepared by ion-exchange reaction and subsequent photo-induced reduction method showed even higher photocatalytic activity than Ag@AgCl under visible light irradiation. The higher photocatalytic efficiency of AgBr might be due to the lower electron affinity of Br^0 than that of Cl^0, making it easier for Br^- to combine with a hole, as well as the smaller band gap of AgBr compared to AgCl.[40] Moreover, the quick absorption of MO molecule on the photocatalyst arising from the complexation of Ag^+ ions with N in the MO molecules, played another important role in the fast degradation rate.[41] Given that AgBr could also be directly excited by visible light, a new insight into the photocatalytic mechanism of Ag@AgBr involving interesting synergistic effect between plasmonic Ag photocatalysis and the conventional AgBr-based semiconductor photocatalysis was proposed by Jiang and coworkers.[42] Under daylight illumination, SPR-excited electrons could be produced and enriched at the surface of Ag NPs. The increased electron density lifted the Fermi energy level of Ag, and the SPR electrons spontaneously transferred from Ag NPs to the CB of AgBr. On the other hand, it was suggested that the synergistic effect arising from SPR-induced local electric field

enhancement in the Ag NPs could accelerate the formation of electron-hole pairs in the semiconductor.[43-44] In this case, more electrons were generated in the CB of AgBr under daylight irradiation. These photo-generated electrons in AgBr, together with the injected SPR electrons from Ag NPs, could then initiate the catalytic reaction, and hence enhanced photocatalytic activity was achieved.

Similarly, a plasmonic photocatalyst Ag-AgI supported on an insulating solid mesoporous alumina (Ag-AgI/Al_2O_3) was prepared by Hu and coworkers.[45] They first deposited AgI on Al_2O_3 support by a deposition-precipitation method, and then reduced some Ag^+ ions on the surface of AgI particles to produce Ag NPs via a photocatalytic reduction method. The photocatalytic activity of AgI/Al_2O_3 was greatly enhanced when it was further loaded with Ag NPs. Under visible light irradiation, the obtained Ag-AgI/Al_2O_3 photocatalyst could effectively degrade the pollutant phenolic compounds including 2-chlorophenol (2-CP), 2,4-dichlorophenol (2,4-DCP) and trichlorophenol (TCP). The plasmonic photocatalytic mechanism was proposed based on a two-electron transfer process from the plasmon-excited Ag NPs to AgI and from 2-CP to the Ag NPs. It should be mentioned that, the transfer of SPR electrons to the CB of AgBr[42] or AgI[45] was quite different from other reports in the case of Ag@AgBr plasmonic photocatalyst,[40-41] where the photo-generated electrons were supposed to enrich on the Ag NPs and be far away from AgBr to prevent the reduction of Ag^+ in AgBr, according to the self-stability mechanism. More studies are still needed to elucidate the photocatalytic mechanism of these photocatalysts.

Although many kinds of Ag@Ag salts have been proved to be promising candidates for the development of visible-light photocatalysts with high efficiency, the photocatalytic properties of this kind of catalysts closely depend on the type of the Ag salts, namely, the photocatalytic activities can be tuned by altering the anions of the

Ag salts. In order to understand how the photocatalyst performance of the Ag salts depends on the negatively charged ions in their salts, Huang et al. designed and fabricated a series of Ag@Ag salts photocatalysts with different anions, such as Cl^-, Br^-, I^-, CrO_4^{2-}, PO_4^{3-}, $PW_{12}O_{40}^{3-}$ and $SiW_{12}O_{40}^{4-}$.[46] They systematically compared the photocatalytic performance of these catalysts in decomposition of MO under visible light illumination, and concluded that higher stability and higher charged anions leaded to the stronger photocatalytic ability.

3.2 Morphology control of Ag-based photocatalysis

Given that the photocatalytic reactions are typically surface-based processes, the performance of the semiconductor materials is strongly dependent on their morphologies. Therefore, it would be a promising way to further improve the photocatalytic activity by shape-controlled synthesis of photocatalytic materials. Because of the distinct electronic, optical and chemical properties, one-dimensional (1-D) nanostructures (including wires, belts, rods and tubes) have received considerable attention for photocatalytic applications.[47-50] Among them, 1-D coaxial hetero-nanostructures with modulated compositions and interfaces have attracted particular interest because of their synergetic effects on the enhancement of photocatalytic performance.[51-52] Recently, Wang et al. synthesized Ag/AgCl core-shell nanowire heterostructures through in situ oxidation of Ag nanowires by $FeCl_3$ (Fig. 3A and 3C).[53] The obtained Ag/AgCl core-shell nanowires could efficiently decompose MO dye under visible light irradiation, and the optimized ratio of Ag to AgCl was 8:92 for the best photocatalytic activity. Moreover, the AgCl nanowires could be feasibly modified with Au NPs (Fig. 3D-F).[54] The Au NPs were generated from the reduction of Au precursor by Fe^{2+}, which was derived from the reduction of

$FeCl_3$ by Ag nanowires. The formed Au NPs on the surface of AgCl nanowires enhanced the stability and the visible light absorption, and the resulting composite AgCl:Au nanowires exhibited good photocatalytic activity toward decomposition of MB dye under visible light illumination.

In addition, redox reactions involving Ag nanowires have also been employed to synthesize novel 2-D dendritic Ag_3PO_4 nanostructures. For example, Bi et al. produced 2-D dendritic Ag_3PO_4 nanostructures by directly reacting Ag nanowires with H_2O_2 and Na_2HPO_4 in aqueous solution at room temperature.[55] They used poly(vinylpyrrolidone) (PVP) as the capping agent, which selectively adsorbed on the surfaces of Ag_3PO_4 nanoclusters, and thus changed their growth direction. Both PVP and Ag nanowires played crucial roles in successful preparation of dendritic Ag_3PO_4 nanostructures. Under visible light irradiation, the novel 2-D dendritic Ag_3PO_4 exhibited much higher photocatalytic activities compared to irregular Ag_3PO_4 nanocrystals and N-doped TiO_2 catalyst for the degradation of RhB dye.[55]

In addition to the role as facile templates for the preparation of novel nanostructures, Ag nanowires can also be used to couple with semiconductor materials to further enhance the charge separation efficiency due to their high conductivity. For instance, the necklace-like hetero-photocatalysts have been constructed by selectively growing Ag_3PO_4 submicro-cubes on Ag nanowires.[56] As shown in the SEM image in Fig. 4A, the single-crystal Ag nanowire drilled through the two parallel {100} facets of each Ag_3PO_4 submicro-cube and joined them together along the longitudinal axis. The density of Ag_3PO_4 cubes on Ag nanowires could be readily tailored by adjusting the concentration of $[Ag(NH_3)_2]^+$ complex (Fig. 4B-D). This novel hetero-structure with proper Ag_3PO_4 density exhibited much higher activities than both pure Ag_3PO_4 cubes and Ag nanowires towards the degradation of

RhB (Fig. 4E) and MO (Fig. 4F) under visible light irradiation.

In addition to the studies described above, porous micro- or nano-structured materials with unique properties, such as large surface areas, low density, surface permeability, and light-trapping effects, have been widely applied in various fields.[57-58] The porous structures may be beneficial to photocatalytic process because of more active sites, and less resistance to mass transfer in the reaction.[59] Very recently, Liang et al. synthesized uniform hierarchical Ag_3PO_4 porous microcubes by a one-step reaction.[60] In their study, trisodium citrate was used as structure directing agent, crystal growth modifier and aggregation-orienting agent in the formation of porous microstructure. Under the irradiation of visible light, the porous Ag_3PO_4 microcubes exhibited superior photocatalytic performance for decomposing RhB as compared to those of solid Ag_3PO_4 particles and commercial P25 TiO_2 powders. They claimed that the narrow bandgap, large surface-to-volume ratio, more active sites and synergistic effect of hierarchical porous structure contributed to the enhanced photocatalytic activity. Moreover, porous Ag_2S-Ag heterostructure nanotubes were successfully prepared by a one-pot microwave-assisted method (Fig. 5A-C).[20] The Ag content in the composite significantly influenced the photocatalytic performance, which could be easily tuned by varying the thioacetamide concentration. The as-prepared hybrid structures with a moderate Ag_2S/Ag molar ratio displayed excellent photocatalytic activity for degradation of MO (Fig. 5D) and reduction of aqueous Cr^{VI} (Fig. 5E) under visible light irradiation.

3.3 Facet-controlled engineering of Ag-based photocatalysis

On the other hand, different facets of a single crystal possess distinctive chemical and physical properties, and the exposed highly reactive facets generally exhibit much

higher catalytic activities.[61] For example, the highly active facet {001} of TiO_2 crystals exhibited significantly greater photocatalytic performance than other common stable facets. The photocatalytic activities of TiO_2 crystals could be tuned by varying the percentage of {001} facet, and TiO_2 with a higher percentage of {001} facet exhibited more effective photocatalytic performance.[62] Nevertheless, the high energy surfaces diminished rapidly during the crystal growth process in order to minimize surface energy. Generally, it is favorable to introduce some certain ions or surfactants for the formation of highly reactive facets, which can markedly reduce the surface energy in the crystal growth process. For example, Wang et al. developed a facile precipitation reaction by using PVP as a capping agent for the synthesis of AgBr nanoplates with exposed {111} facet.[63] They found that both of the AgBr-based photocatalysts showed better photocatalytic performance than Ag_3PO_4 under visible light irradiation, and the rate of MO decomposition over AgBr nanoplates was four times faster than irregular AgBr particles. The enhanced photocatalytic activities of AgBr/Ag nanoplates were explained rationally by the density functional theory calculation results, which showed that the surface energy of the AgBr {111} surface (ca. 1.253 J/m^2) was higher than that of AgBr {100} (ca. 0.495 J/m^2) and {110} (ca. 0.561 J/m^2). This result indicated that the {111} facet of AgBr was more reactive than {110} and {100}, and thus was very favorable for enhancing the photocatalytic activity. In addition, the five distinct morphologies of Ag_2O microcrystals, including cubic, octahedral, rhombic dodecahedral, rhombicuboctahedral and polyhedra with 18 faces, were successfully prepared by controlling the type or concentration of complexing agents.[64] Under the visible light illumination, they exhibited facet-dependent photocatalytic activities for the degradation of MO dye, and the order of degradation rate was in accordance with that of the Ag_2O surface energies ({100} >

{110} > {111}). The cubic Ag_3PO_4 crystals were also proved to possess higher catalytic activity and photoelectric property than spherical particles for degradation of MB dye and photoelectric conversion under visible light irradiation, which might be attributed to their novel cubic structure and exposed {100} facets.[65]

The capping agents adsorbed on the semiconductor crystals is another factor to be considered because they masked the reactive surface and have to be removed before the photocatalytic applications. Therefore, it is desirable to develop controlled synthesis methods for semiconductor materials with exposed reactive facets and clean surface. Successful examples for the synthesis of photocatalysts with highly reactive facets exposed but without capping agents were reported recently. Ye and co-workers fabricated two forms of single-crystalline Ag_3PO_4, i.e., the rhombic dodecahedrons enclosed by 12 well-defined {110} facets (Fig. 6A) and the cubes bounded by {100} facets (Fig. 6B), by using CH_3COOAg and $[Ag(NH_3)_2]^+$ complex as the silver ion precursors in aqueous solutions at room temperature, respectively.[66] The rhombic dodecahedral Ag_3PO_4 exhibited higher photocatalytic activity for the degradation of MO and RhB dyes than the cubes under the identical conditions, indicating the {110} facet was more reactive than the {100} facet. The result was consistent with the higher surface energy of 1.31 J/m^2 of {110} facet compared to 1.12 J/m^2 of {100} facet. Moreover, the tetrapod-shaped Ag_3PO_4 microcrystals (Fig. 6C-D) with an increased percentage of exposed {110} facets were prepared through a facile precipitation route in aqueous solution[67] or simple hydrothermal method[68] without any surfactant. The Ag_3PO_4 microcrystals were three-dimensional tetrapods, and the arms were hexagonal prisms. Under visible light irradiation, both Ag_3PO_4-based photocatalysts exhibited obvious superior photocatalytic performance to the reference N-TiO_2, and the photodegradation rate of MO and RhB dyes over Ag_3PO_4 tetrapods

was faster than that of irregular Ag_3PO_4 particles. In addition, tetrahedral submicro-crystals (Fig. 6E),[69] and concave trisoctahedral Ag_3PO_4 microcrystals (Fig. 6F)[70] were also synthesized and exhibited the enhanced photocatalytic performance.

3.4 Composite photocatalysts

Semiconductor photocatalysis could be regarded as a type of system engineering, and a series of tasks such as optoelectronic conversion, electrons and holes separation, surface/interface catalysis, mass transfer (such as adsorption/desorption, diffusion, etc.), and post-treatment or recycling of the photocatalyst should be involved. Thus, all the relevant functions need to be optimized into the photocatalytic system. However, it is hard to fulfill all the tasks mentioned above satisfactorily by a single composition. Therefore, combining with other advanced materials to design the composite photocatalysts with integrated function might be a promising way.

In order to facilitate the electron-hole pair separation in semiconductor photocatalysts to further improve their photoelectrochemical activities, numerous studies have recently been performed to organize the semiconductor-semiconductor composite hierarchical structures.[71-72] Among a wide spectrum of the semiconductor photocatalysts, TiO_2 and ZnO are still by far the most widely used photocatalysts because of their excellent properties such as high photocatalytic efficiency, good stability, low cost, nontoxicity and so on. The main drawback of these conventional photocatalysts is the lack of visible light utilization due to their large band gap. To overcome this problem, many attempts have been made to enhance the photocatalytic efficiency and visible light utilization by combining with narrow band gap semiconductors.[73-76] Recently, researchers found that, Ag-based compounds such as Ag_2O, AgX (X=Cl, Br, I), and Ag_3PO_4, are excellent candidates to couple with TiO_2

or ZnO, which effectively improve photocatalytic efficiency of these conventional photocatalysts. The synergetic effects on both carrier separation and photocatalytic efficiency in such heterostructures have been studied in recent years. In most cases, the Ag-based compounds serve as a visible light sensitizer, which promote the interfacial electron transfer process and thus reduce the charge recombination in the semiconductor. Typical examples of such systems include Ag_2O/TiO_2,[77] Ag_2O/ZnO,[78] AgX/TiO_2,[79-82] AgX/ZnO,[83-85] Ag_3PO_4/TiO_2,[86] Ag_3PO_4/ZnO,[87] Ag_3VO_4/TiO_2,[88] and so on.

Besides the conventional large band gap semiconductors such as TiO_2 and ZnO, some small band gap semiconductors such as Bi_2O_3,[89] $Bi_{20}TiO_{32}$,[90] $BiVO_4$,[91] BiOX (X=Cl, Br)[92] and WO_3[93] have also been incorporated with Ag-based high-efficient photocatalysts to construct hierarchical photocatalysts. Due to the efficient separation and transfer of photogenerated electron-hole pairs between these two semiconductors, all the hierarchical photocatalysts with optimized mass ratio have superior photocatalytic performance compared to each single semiconductor-based photocatalyst.

Moreover, the Ag-based semiconductor composite hierarchical nanostructures also exhibit significantly improved stability. For example, enhanced photocatalytic properties and stabilities were achieved by the epitaxial growth of AgX (X = Cl, Br, I) nanoshells on the surfaces of rhombic dodecahedral Ag_3PO_4 crystals.[94] In AgX/Ag_3PO_4 core-shell heterostructures, the AgX nanoshell was in intimate contact with the outer surfaces of Ag_3PO_4 crystals. Because AgX nanoshell was much less soluble in an aqueous solution, it could effectively protect the Ag_3PO_4 core-crystals from dissolution during the photocatalytic process. Thus, their structural stabilities were greatly improved. In addition, the energy bands of AgX semiconductors (with an

exception of AgCl) and Ag_3PO_4 crystals matches, which could promote the transfer and separation of photo-excited electron-hole pairs through the hetero-junctions. Similarly, this strategy for enhancing efficiency and the stability of photocatalysts were also applied to $AgBr/Ag_2CO_3$ hybrid materials.[95]

In addition to the photocatalysts mentioned above, the cheap and abundant carbon materials (carbon nanotubes, graphene and its derivatives, carbon quantum dots) have been also introduced to enhance the photoelectrochemical activity of Ag-compound based photocatalysts due to their unique structure and remarkable properties. Carbon nanotubes (CNTs) are 1-D structures based on carbon layers with sp^2 bonds rolled into cylindrical tubes. It has been frequently employed as a catalyst carrier owing to its hollow structure as well as its large specific surface area.[96-97] Additionally, CNTs could serve as an electron attracting reservoir to reduce the electron-hole recombination, and hence improve the performance of the resultant composite photocatalysts.[98] Recently, Xu et al. synthesized the CNTs-loaded Ag/AgBr by a simple one-step hydrothermal method.[99] The obtained CNT/Ag/AgBr hybrid composite with low CNT content ($<$4.1 at%) showed better photocatalytic ability for the degradation of MO dye than pure Ag/AgBr. Subsequently, Ag/AgX (X= Cl, Br, I) loaded on CNTs composites with improved photoactivity for 2,4,6-tribromophenol (TBP) degradation in aqueous phase under visible light was prepared.[100] The main reason for the photocatalytic performance enhancement was attributed to the loaded CNTs, which promoted the separation of electron-hole pairs in the hybrid photocatalysts. Furthermore, Zhai et al. developed a new kind of photocatalytic system based on Pickering emulsions.[101] The Pickering emulsions were formed by self-assembling Ag_3PO_4-multiwalled carbon nanotubes (MWNTs) nanohybrid at the water/oil interface (Fig. 7A). Under visible light irradiation, the as-formed

photocatalytic system exhibited superior photocatalytic capability compared to raw Ag_3PO_4 nanoparticles in the solution for the decomposition of MB dyes (Fig. 7B), as well as for the evolution of O_2 from water (Fig. 7C). It was elucidated that the excellent features of Pickering emulsions (including enlarged active surface area, facilitated separation of products from reactants at the water/oil interface), together with promoted charge separation by CNTs, contributed to the enhanced photocatalytic activity.[101]

Another more popular carbonaceous material, graphene, has attracted a lot of attention since its discovery because of its outstanding mechanical, thermal, optical, and electrical properties. Recently, numerous attempts have been attempted to design and prepare graphene-based semiconductor photocatalysts.[102-103] In particular, some works have been made to combine graphene or graphene oxide (GO) with Ag-containing compounds to enhance their photocatalytic performance. For instance, the GO enwrapped Ag/AgX (X= Br, Cl) nanocomposites were prepared in an oil/water system at room temperature and used as one kind of highly efficient visible-light plasmonic photocatalysts (Fig. 8A-C).[104] The improved adsorption affinity of Ag/AgX/GO towards MO molecules was achieved by hybridization of Ag/AgX with GO nanosheets, owing to the non-covalent intermolecular π-π interactions between the MO molecules and GO-based hybrids. These hybrid photocatalysts exhibited better visible-light photocatalytic activities for degradation of MO dyes compared to the bare Ag/AgX composite (Fig. 8 D-E). Similarly, the graphene sheets grafted Ag@AgCl composite was prepared via deposition-precipitation reaction and followed by photoreduction method.[105] Under visible light irradiation, the composite catalyst displayed a four-fold enhancement in the photodegradation of RhB compared to bare Ag/AgCl nanoparticles. The obvious

enhancement of photocatalytic activity was attributed to the effective charge transfer from SPR-excited Ag NPs to GO, which suppressed the charge recombination during photocatalytic process. In addition, composites of other Ag-based photocatalysts and graphene or GO such as Ag_2O-GO,[106] Ag_3PO_4-GO,[107-110] Ag_3PO_4-graphene[111-112] have also been prepared and used as efficient visible-light responsive photocatalysts for the decomposition of organic pollutants in water. The improved photocatalytic activity was mainly attributed to the enlarged surface area, enhanced adsorption of organic substance, and more efficient separation of photogenerated electron-hole pairs. Moreover, the presence of graphene or GO sheets could effectively tailor the size of the Ag-compound particles, and smaller particles were generally obtained in these hybrid composites.[104-105, 110-111] The smaller size of the Ag-compound particles in composites facilitated charge transfer and hence suppressed recombination of electron-hole pairs, which also contributed to the enhanced photocatalytic performance.

Very recently, carbon quantum dots (CQDs) were introduced into Ag_3PO_4 photocatalyst for photocatalytic decomposition of MO in water under visible light irradiation.[113] In comparison to Ag_3PO_4 particles, both CQDs/Ag_3PO_4 and CQDs/Ag/Ag_3PO_4 displayed enhanced photocatalytic activities and good structural stabilities. The improved efficiency could be attributed to three effects. First, the dissolution and photocorrosion of Ag_3PO_4 could be prevented by CQDs on the surface of Ag_3PO_4 based on their insolubility and photoinduced electron transfer properties. Second, the excellent upconverted photoluminescence behavior of CQDs enables the complex systems to effectively utilize the full spectrum of sunlight. Finally, CQDs could act as an electron reservoir to facilitate the transport of the photogenerated electrons, and thus hinder the electron-hole pair recombination in the coupling

system.

As well known, reducing the size of photocatalyst is generally beneficial for surface-dependent photocatalysis because it leads to higher specific surface area and hence more reactive sites. The emergence of nano-photocatalyst has offered efficient ways for promoting photocatalytic efficiency.[36] In the nano-photocatalyst system, carriers migrating to the surface have extremely short distances to travel and, as a result, reduce the recombination possibility for photo-excited electron-hole pairs. For example, the Ag_3PO_4 nanocrystals with particle size ranging from 8 to 16 nm possessed superior catalytic activity in the photodecomposition of MB under visible light irradiation as compared to Ag_3PO_4 microcrystals.[114] However, for the practical applications in aqueous media, the recycling of nano-sized photocatalysts from the reaction system is an important but remains extremely difficult due to the small size of the catalysts employed. One feasible solution is to develop magnetic photocatalytic materials. Recently, Li et al. reported a facile and fast approach for the synthesis of magnetically separable Ag_3PO_4-Fe_3O_4 sub-micrometre composites.[115] These composites could effectively decompose MB dye under visible light irradiation, which could be collected by an external magnet after the reaction and reused for the next cycle. In addition, Ag-AgX/Fe_3O_4@SiO_2 (X=Cl, Br or I) was also prepared by immobilizing photocatalytically active components on silica-coated magnetic Fe_3O_4 nanoparticles.[116-118] They exhibited enhanced performance towards the decomposition of organic molecules under visible light illumination, and could be easily recovered owing to their paramagnetic property.

4. Conclusion and perspectives

In summary, we have summarized recent developments on engineering a series of

Ag-containing compounds such as Ag_2O, Ag_2S, AgX (X=Cl, Br, I), Ag_2CO_3, Ag_3PO_4 and so forth as highly efficient photocatalysts for decomposing organic substance under the illumination of visible light or sunlight. The photocatalytic performance could be rationally tuned through morphology and facet-controlled processes. Furthermore, by combining with other functional materials, Ag-compound based hybrids show even better photocatalytic activities because these additional functional materials can introduce new or improved properties such as extended light absorption, enhanced charge separation and transportation properties, enhanced structure stability, improved adsorption affinity, and enhanced solar energy conversion.

Ag-compound based photocatalysts have attracted extensive attention due to their high photocatalytic activities under visible light irradiation and potential applications in environmental remediation. Although considerable advances in this area have already been made over the past a few years, the studies in this field are still at the initial stage. A number of challenges still exist and further developments of more Ag-based photocatalysts are required. First, Ag salts are unstable under irradiation. Although the self-stability mechanism of Ag/Ag salts under illumination has been proposed and supported by some experimental evidences, the distribution of the Ag NPs on the surface of Ag salts and the exact proportion of metallic Ag to stabilize the composite are not clear. Moreover, the size, shape and ratio of Ag NPs in the composite significantly influence the photocatalytic performance. Thus, facile reduction method needs to be developed to realize the size, shape and number control of Ag NPs in the formation process. Second, the detailed mechanism of the photocatalytic reaction is still unclear, and the proposed possible mechanism is under debate. More works as well as theoretical investigations should be done to obtain a better understanding of the photocatalytic process on these Ag-based compounds.

Third, the scarcity and high cost of Ag salts would be an obvious limitation in practical applications. How to fully realize the high performance photocatalysis and make the catalysts robust and easily recovered from the reaction system for repeated use are important issues. Nevertheless, the development of the exploration of Ag-compound based materials for photocatalytic applications is quite fast nowadays, and we believe the present challenges will be gradually overcome. Furthermore, the rapid development of materials science over the past a few years have created many kinds of advanced materials. By incorporating these advanced materials with Ag-compound photocatalysts, the performance of the catalysts will be largely improved.

Acknowledgement

This work was financially supported by the NSF of China (21210007, 91213305, and 91232000 for L.M., and 21305129 for G. L.), the National Basic Research Program of China (the 973 programs 2010CB33502), and Chinese Academy of Sciences.

References

1. A. Vaseashta, M. Vaclavikova, S. Vaseashta, G. Gallios, P. Roy and O. Pummakarnchana, *Sci. Technol. Adv. Mat.,* 2007, **8**, 47-59.
2. D. Leštan, C. L. Luo and X. D. Li, *Environ. Pollut.,* 2008, **153**, 3-13.
3. N. S. Lewis and D. G. Nocera, *Proc. Natl. Acad. Sci.,* 2006, **103**, 15729-15735.
4. M. Grätzel, *Acc. Chem. Res.,* 2009, **42**, 1788-1798.
5. J. L. Dempsey, A. J. Esswein, D. R. Manke, J. Rosenthal, J. D. Soper and D. G. Nocera, *Inorg. Chem.,* 2005, **44**, 6879-6892.
6. A. Fujishima and K. Honda, *Nature,* 1972, **238**, 37-38.
7. J.-M. Herrmann, *Catal. Today,* 1999, **53**, 115-129.
8. U. I. Gaya and A. H. Abdullah, *J. Photochem. Photobiol. C: Photochemistry Reviews,* 2008, **9**, 1-12.
9. X. Chen, S. Shen, L. Guo and S. S. Mao, *Chem. Rev.,* 2010, **110**, 6503-6570.
10. M. Anpo and M. Takeuchi, *Int. J. Photoenergy,* 2001, **3**, 89-94.
11. R. Asahi, T. Morikawa, T. Ohwaki, K. Aoki and Y. Taga, *Science,* 2001, **293**, 269-271.
12. S. In, A. Orlov, R. Berg, F. García, S. Pedrosa-Jimenez, M. S. Tikhov, D. S. Wright and R. M. Lambert, *J. Am. Chem. Soc.,* 2007, **129**, 13790-13791.
13. X. Chen and C. Burda, *J. Am. Chem. Soc.,* 2008, **130**, 5018-5019.
14. Z. Zheng, B. Huang, X. Qin, X. Zhang, Y. Dai and M. H. Whangbo, *J. Mater. Chem.,* 2011, **21**, 9079-9087.
15. W. Smith, A. Wolcott, R. C. Fitzmorris, J. Z. Zhang and Y. Zhao, *J. Mater. Chem.,* 2011, **21**, 10792-10800.
16. D. R. Baker and P. V. Kamat, *Adv. Funct. Mater.,* 2009, **19**, 805-811.
17. P. Yu, K. Zhu, A. G. Norman, S. Ferrere, A. J. Frank and A. J. Nozik, *J. Phys. Chem. B,* 2006, **110**, 25451-25454.
18. W. Kim, T. Tachikawa, T. Majima and W. Choi, *J. Phys. Chem. C,* 2009, **113**, 10603-10609.
19. X. Wang, S. Li, H. Yu, J. Yu and S. Liu, *Chem. A Euro. J.,* 2011, **17**, 7777-7780.

20. W. Yang, L. Zhang, Y. Hu, Y. Zhong, H. B. Wu and X. W. D. Lou, *Angew. Chem. Int. Ed.,* 2012, **51**, 11501-11504.
21. P. Wang, B. Huang, X. Qin, X. Zhang, Y. Dai, J. Wei and M. H. Whangbo, *Angew. Chem. Int. Ed.,* 2008, **47**, 7931-7933.
22. C. An, S. Peng and Y. Sun, *Adv. Mater.,* 2010, **22**, 2570-2574.
23. P. Wang, B. Huang, Q. Zhang, X. Zhang, X. Qin, Y. Dai, J. Zhan, J. Yu, H. Liu and Z. Lou, *Chem. A Euro. J.,* 2010, **16**, 10042-10047.
24. H. Dong, G. Chen, J. Sun, C. Li, Y. Yu and D. Chen, *Appl. Catal. B: Environmental,* 2013, **134-135**, 46-54.
25. Z. Yi, J. Ye, N. Kikugawa, T. Kako, S. Ouyang, H. Stuart-Williams, H. Yang, J. Cao, W. Luo and Z. Li, *Nat. Mater.,* 2010, **9**, 559-564.
26. N. Kakuta, N. Goto, H. Ohkita and T. Mizushima, *J. Phys. Chem. B,* 1999, **103**, 5917-5919.
27. P. V. Kamat, *J. Phys. Chem. B,* 2002, **106**, 7729-7744.
28. K. L. Kelly, E. Coronado, L. L. Zhao and G. C. Schatz, *J. Phys. Chem. B,* 2003, **107**, 668-677.
29. D. B. Ingram, P. Christopher, J. L. Bauer and S. Linic, *ACS Catal.,* 2011, **1**, 1441-1447.
30. T. Hirakawa and P. V. Kamat, *J. Am. Chem. Soc.,* 2005, **127**, 3928-3934.
31. A. Primo, T. Marino, A. Corma, R. Molinari and H. Garcia, *J. Am. Chem. Soc.,* 2011, **133**, 6930-6933.
32. A. Primo, A. Corma and H. García, *Phys. Chem. Chem. Phys.,* 2011, **13**, 886-910.
33. S. Sarina, E. R. Waclawik and H. Zhu, *Green Chem.,* 2013, **15**, 1814-1833.
34. G. Dai, J. Yu and G. Liu, *J. Phys. Chem. C,* 2012, **116**, 15519-15524.
35. N. Umezawa, O. Shuxin and J. Ye, *Phys. Rev. B,* 2011, **83**, 035202.
36. H. Tong, S. Ouyang, Y. Bi, N. Umezawa, M. Oshikiri and J. Ye, *Adv. Mater.,* 2012, **24**, 229-251.
37. X. Jin, I. Y. Kim, Y. K. Jo, J. L. Bettis, H. J. Koo, M. H. Whangbo and S. J. Hwang, *J. Phys. Chem. C,* 2013, **117**, 26509-26516.

38. C. An, R. Wang, S. Wang and X. Zhang, *J. Mater. Chem.,* 2011, **21**, 11532-11536.

39. H. Xu, H. Li, J. Xia, S. Yin, Z. Luo, L. Liu and L. Xu, *ACS Appl. Mater. Interfaces,* 2010, **3**, 22-29.

40. P. Wang, B. Huang, X. Zhang, X. Qin, H. Jin, Y. Dai, Z. Wang, J. Wei, J. Zhan, S. Wang, J. Wang and M. H. Whangbo, *Chem. A Euro. J.,* 2009, **15**, 1821-1824.

41. L. Kuai, B. Geng, X. Chen, Y. Zhao and Y. Luo, *Langmuir,* 2010, **26**, 18723-18727.

42. J. Jiang , H. Li and L. Zhang, *Chem. A Euro. J.,* 2012, **18**, 6360-6369.

43. P. Christopher, D. B. Ingram and S. Linic, *J. Phys. Chem. C,* 2010, **114**, 9173-9177.

44. D. B. Ingram and S. Linic, *J. Am. Chem. Soc.,* 2011, **133**, 5202-5205.

45. C. Hu, T. Peng, X. Hu, Y. Nie, X. Zhou, J. Qu and H. He, *J. Am. Chem. Soc.,* 2009, **132**, 857-862.

46. H. Huang, X. Li, Z. Kang, Y. Liu, H. Li, X. He, S. Lian, J. Liu and S. T. Lee, *Dalton Trans.,* 2010, **39**, 10593-10597.

47. T. J. Kuo, C. N. Lin, C. L. Kuo and M. H. Huang, *Chem. Mater.,* 2007, **19**, 5143-5147.

48. J. Jitputti, Y. Suzuki and S. Yoshikawa, *Catal. Commun.,* 2008, **9**, 1265-1271.

49. Y. Wang, L. Zhang, K. Deng, X. Chen and Z. Zou, *J. Phys. Chem. C,* 2007, **111**, 2709-2714.

50. Y. Chen, J. C. Crittenden, S. Hackney, L. Sutter and D. W. Hand, *Environ. Sci. Technol.,* 2005, **39**, 1201-1208.

51. M. Shahid, I. Shakir, S.-J. Yang and D. J. Kang, *Mater. Chem. Phys.,* 2010, **124**, 619-622.

52. J. Xiong, Z. Li, J. Chen, S. Zhang, L. Z. Wang and S. X. Dou, *ACS Appl. Mater. Interfaces,* 2014,

53. Y. Bi and J. Ye, *Chem. Commun.,* 2009, 6551-6553.

54. Y. Sun, *J. Phys. Chem. C,* 2010, **114**, 2127-2133.

55. Y. Bi, H. Hu, Z. Jiao, H. Yu, G. Lu and J. Ye, *Phys. Chem. Chem. Phys.,* 2012, **14**,

14486-14488.

56. Y. Bi, H. Hu, S. Ouyang, Z. Jiao, G. Lu and J. Ye, *J. Mater. Chem.,* 2012, **22**, 14847–14850.
57. M. E. Davis, *Nature,* 2002, **417**, 813-821.
58. A. Wittstock, V. Zielasek, J. Biener, C. Friend and M. Bäumer, *Science,* 2010, **327**, 319-322.
59. Y. Zhao, X. Zhang, J. Zhai, J. He, L. Jiang, Z. Liu, S. Nishimoto, T. Murakami, A. Fujishima and D. Zhu, *Appl. Catal. B: Environmental,* 2008, **83**, 24-29.
60. Q. Liang, W. Ma, Y. Shi, Z. Li and X. Yang, *Crystengcomm,* 2012, **14**, 2966-2973.
61. A. Selloni, *Nat. Mater.,* 2008, **7**, 613-615.
62. X. Han, Q. Kuang, M. Jin, Zhaoxiong Xie and L. Zheng, *J. Am. Chem. Soc.,* 2009, **131**, 3152-3153.
63. H. Wang, J. Gao, T. Guo, R. Wang, L. Guo, Y. Liu and J. Li, *Chem. Commun.,* 2012, **48**, 275-277.
64. G. Wang, X. Ma, B. Huang, H. Cheng, Z. Wang, J. Zhan, X. Qin, X. Zhang and Y. Dai, *J. Mater. Chem.,* 2012, **22**, 21189-21194.
65. Y. Bi, H. Hu, S. Ouyang, G. Lu, J. Cao and J. Ye, *Chem. Commun.,* 2012, **48**, 3748-3750.
66. Y. Bi, S. Ouyang, N. Umezawa, J. Cao and J. Ye, *J. Am. Chem. Soc.,* 2011, **133**, 6490-6492.
67. H. Wang, L. He, L. Wang, P. Hu, L. Guo, X. Han and J. Li, *Crystengcomm,* 2012, **14**, 8342-8344.
68. J. Wang, F. Teng, M. Chen, J. Xu, Y. Song and X. Zhou, *Crystengcomm,* 2013, **15**, 39-42.
69. H. Hu, Z. Jiao, H. Yu, G. Lu, J. Ye and Y. Bi, *J. Mater. Chem. A,* 2013, **1**, 2387-2390.
70. Z. Jiao, Y. Zhang, H. Yu, G. Lu, J. Ye and Y. Bi, *Chem. Commun.,* 2013, **49**, 636-638.
71. J. C. Tristão, F. Magalhães, P. Corio and M. T. C. Sansiviero, *J. Photochem.*

Photobiol. A: Chem., 2006, **181**, 152-157.

72. S. Yan, S. Lv, Z. Li and Z. Zou, *Dalton Trans.,* 2010, **39**, 1488-1491.
73. G. S. Li, D. Q. Zhang and J. C. Yu, *Environ. Sci. Technol.,* 2009, **43**, 7079-7085.
74. X. Li, H. Liu, D. Luo, J. Li, Y. Huang, H. Li, Y. Fang, Y. Xu and L. Zhu, *Chem. Engineer. J,* 2012, **180**, 151-158.
75. D. Barpuzary, Z. Khan, N. Vinothkumar, M. De and M. Qureshi, *J. Phys. Chem. C,* 2011, **116**, 150-156.
76. P. Kundu, P. A. Deshpande, G. Madras and N. Ravishankar, *J. Mater. Chem.,* 2011, **21**, 4209-4216.
77. W. Zhou, H. Liu, J. Wang, D. Liu, G. Du and J. Cui, *ACS Appl. Mater. Interfaces,* 2010, **2**, 2385-2392.
78. M. Wu, J. M. Yan, M. Zhao and Q. Jiang, *ChemPlusChem,* 2012, **77**, 931-935.
79. M. R. Elahifard, S. Rahimnejad, S. Haghighi and M. R. Gholami, *J. Am. Chem. Soc.,* 2007, **129**, 9552-9553.
80. Y. Hou, X. Li, Q. Zhao, X. Quan and G. Chen, *J. Mater. Chem.,* 2011, **21**, 18067-18076.
81. W. Sun, Y. Li, W. Shi, X. Zhao and P. Fang, *J. Mater. Chem.,* 2011, **21**, 9263-9270.
82. J. F. Guo, B. Ma, A. Yin, K. Fan and W. L. Dai, *J. Hazard. Mater.,* 2012, **211**, 77-82.
83. G. Begum, J. Manna and R. K. Rana, *Chem. A. Eur. J.,* 2012, **18**, 6847-6853.
84. C. Wu, L. Shen, Y. C. Zhang and Q. Huang, *Mater. Lett.,* 2012, **66**, 83-85.
85. K. Vignesh, A. Suganthi, M. Rajarajan and S. Sara, *Powder Technol.,* 2012, **224**, 331-337.
86. W. Yao, B. Zhang, C. Huang, C. Ma, X. Song and Q. Xu, *J. Mater. Chem.,* 2012, **22**, 4050-4055.
87. W. Liu, M. Wang, C. Xu, S. Chen and X. Fu, *Mater. Res. Bull.,* 2013, **48**, 106-113.
88. J. Wang, H. Ruan, W. Li, D. Li, Y. Hu, J. Chen, Y. Shao and Y. Zheng, *J. Phys. Chem. C,* 2012, **116**, 13935-13943.

89. L. Zhu, B. Wei, L. Xu, Z. Lü, H. Zhang, H. Gao and J. Che, *Crystengcomm,* 2012, **14**, 5705-5709.

90. J. Hou, Z. Wang, C. Yang, W. Zhou, S. Jiao and H. Zhu, *J. Phys. Chem. C,* 2013, **117**, 5132-5141.

91. C. Li, P. Zhang, R. Lv, J. Lu, T. Wang, S. Wang, H. Wang and J. Gong, *Small,* 2013, **9**, 3951-3956.

92. L. Ye, J. Liu, C. Gong, L. Tian, T. Peng and L. Zan, *ACS Catal.,* 2012, **2**, 1677-1683.

93. P. Wang, B. Huang, X. Qin, X. Zhang, Y. Dai and M. H. Whangbo, *Inorg. Chem.,* 2009, **48**, 10697-10702.

94. Y. Bi, S. Ouyang, J. Cao and J. Ye, *Phys. Chem. Chem. Phys.,* 2011, **13**, 10071-10075.

95. H. Xu, J. Zhu, Y. Song, W. Zhao, Y. Xu, Y. Song, H. Ji and H. Li, *RSC Adv.,* 2014, **4**, 9139-9147.

96. B. Yoon and C. M. Wai, *J. Am. Chem. Soc.,* 2005, **127**, 17174-17175.

97. G. G. Wildgoose, C. E. Banks and R. G. Compton, *Small,* 2006, **2**, 182-193.

98. J. Yu, T. Ma and S. Liu, *Phys. Chem. Chem. Phys.,* 2011, **13**, 3491-3501.

99. Y. Xu, H. Xu, J. Yan, H. Li, L. Huang, Q. Zhang, C. Huang and H. Wan, *Phys. Chem. Chem. Phys.,* 2013, **15**, 5821-5830.

100. H. Shi, J. Chen, G. Li, X. Nie, H. Zhao, P.-K. Wong and T. An, *ACS Appl. Mater. Interfaces,* 2013, **5**, 6959-6967.

101. W. Zhai, G. Li, P. Yu, L. Yang and L. Mao, *J. Phys. Chem. C,* 2013, **117**, 15183-15191.

102. Q. Xiang, J. Yu and M. Jaroniec, *Chem. Soc. Rev.,* 2012, **41**, 782-796.

103. R. K. Upadhyay, N. Soin and S. S. Roy, *RSC Adv.,* 2014, **4**, 3823-3851.

104. M. Zhu, P. Chen and M. Liu, *ACS Nano,* 2011, **5**, 4529-4536.

105. H. Zhang, X. Fan, X. Quan, S. Chen and H. Yu, *Environ. Sci. Technol.,* 2011, **45**, 5731-5736.

106. Z. Ji, X. Shen, J. Yang, Y. Xu, G. Zhu and K. Chen, *Euro. J. Inor. Chem.,* 2013, **2013**, 6119-6125.

107. Q. Liang, Y. Shi, W. Ma, Z. Li and X. Yang, *Phys. Chem. Chem. Phys.,* 2012, **14**, 15657-15665.

108. L. Liu, J. Liu and D. D. Sun, *Catal. Sci. Technol.,* 2012, **2**, 2525–2532.

109. G. Chen, M. Sun, Q. Wei, Y. Zhang, B. Zhu and B. Du, *J. Hazard. Mater.,* 2013, **244-245**, 86-93.

110. H. Cui, X. Yang, Q. Gao, H. Liu, Y. Li, H. Tang, R. Zhang, J. Qin and X. Yan, *Mater. Lett.,* 2013, **93**, 28-31.

111. B. Jiang, Y. Wang, J. Q. Wang, C. Tian, W. Li, Q. Feng, Q. Pan and H. Fu, *ChemCatChem,* 2013, **5**, 1359-1367.

112. X. Yang, H. Cui, Y. Li, J. Qin, R. Zhang and H. Tang, *ACS Catal.,* 2013, **3**, 363-369.

113. H. Zhang, H. Huang, H. Ming, H. Li, L. Zhang, Y. Liu and Z. Kang, *J. Mater. Chem.,* 2012, **22**, 10501-10506.

114. C. T. Dinh, T. D. Nguyen, F. Kleitz and T. O. Do, *Chem. Commun.,* 2011, **47**, 7797-7799.

115. G. Li and L. Mao, *RSC Adv.,* 2012, **2**, 5108-5111.

116. C. An, X. Ming, J. Wang and S. Wang, *J. Mater. Chem.,* 2012, **22**, 5171-5176.

117. G. Li, K. Wong, X. Zhang, C. Hu, J. C. Yu, R. Chan and P. Wong, *Chemosphere,* 2009, **76**, 1185-1191.

118. J. F. Guo, B. Ma, A. Yin, K. Fan and W. L. Dai, *Appl. Catal. B: Environmental,* 2011, **101**, 580-586.

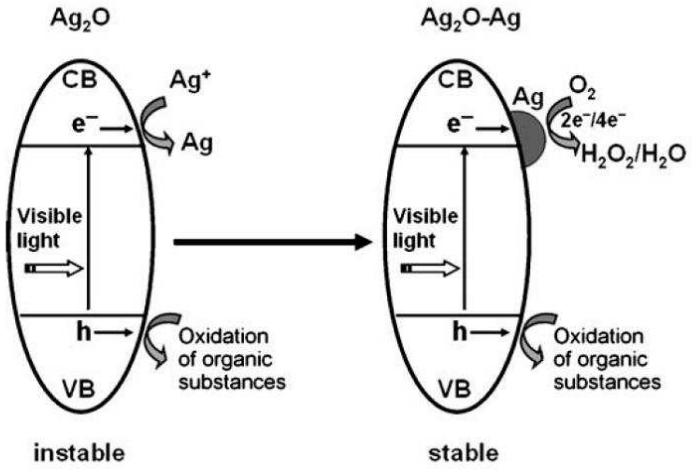

Fig.1 Schematic diagrams showing the self-stabilizing process of the Ag_2O photocatalyst and photocatalytic mechanism under visible light irradiation (h=holes, e^-=electrons) (from ref. 19).

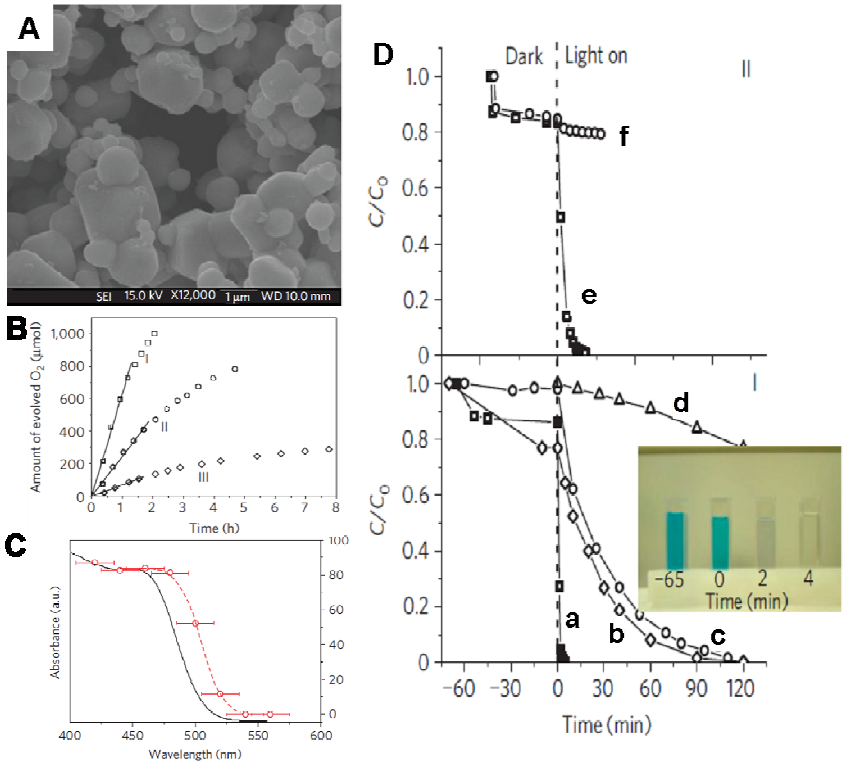

Fig. 2 (A) SEM image of the prepared Ag_3PO_4 powders. (B) O_2 evolution from aqueous $AgNO_3$ solutions under illumination (λ >400 nm) on various semiconductor powders, respectively. (I) Ag_3PO_4: 636 μmol h^{-1}; (II) $BiVO_4$: 246 μmol h^{-1}; (III)WO_3: 72μmol h^{-1}. (C) Ultraviolet-visible diffuse reflectance spectrum and apparent quantum yields of the Ag_3PO_4 semiconductor plotted as a function of wavelength of the incident light. Apparent quantum yields were plotted at the centre wavelengths of the band-pass filters, with error bars showing the deviation of the wavelengths ($\Delta\lambda = \pm 15$ nm). (D) Variation of methylene blue concentration as a function of illumination time under visible light (λ>400 nm) (I) with powder samples Ag_3PO_4 (a), $TiO_{2-x}N_x$ (b), $BiVO_4$ (c) and methylene blue photolysis (d), and under various monochromatic visible lights with Ag_3PO_4 (II) at wavelengths of λ=420.4 nm ($\Delta\lambda = \pm 14.9$ nm) (e) and λ=639.3 nm ($\Delta\lambda = \pm 16.2$ nm) (f). The inset shows the color changes of the methylene blue solutions corresponding to the four filled square points in a (from ref. 25).

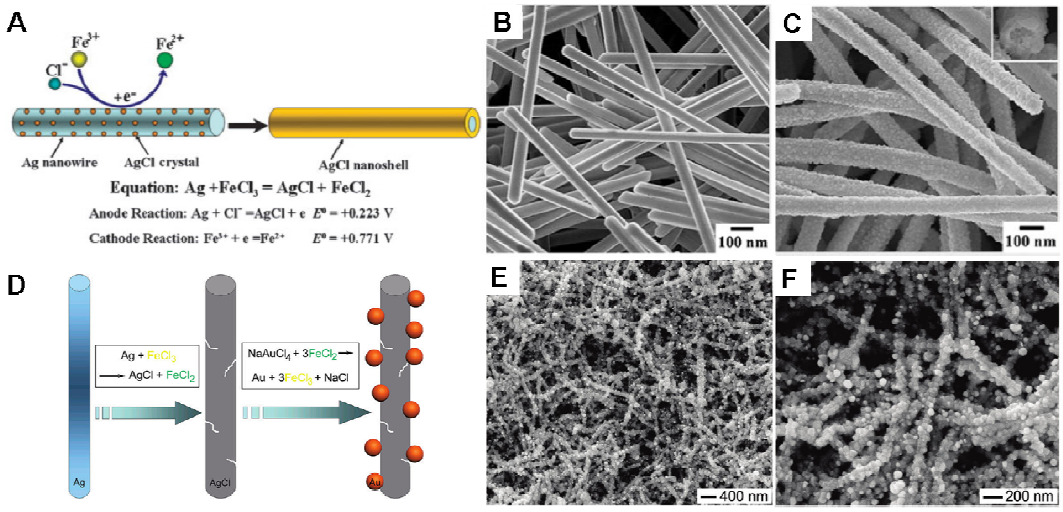

Fig. 3 (A) Schematic illustration of the in situ oxidation process for Ag/AgCl core-shell nanowires. (B, C) SEM images of Ag nanowires and as-prepared Ag/AgCl core-shell nanowires (from ref. 53). (D) Schematic illustration of the major steps involved in the synthesis of AgCl:Au by templating against Ag nanowires (the white lines represent grain boundaries in the AgCl nanowire). (E, F) SEM images of the as-synthesized AgCl:Au nanowires with different magnifications (from ref. 54).

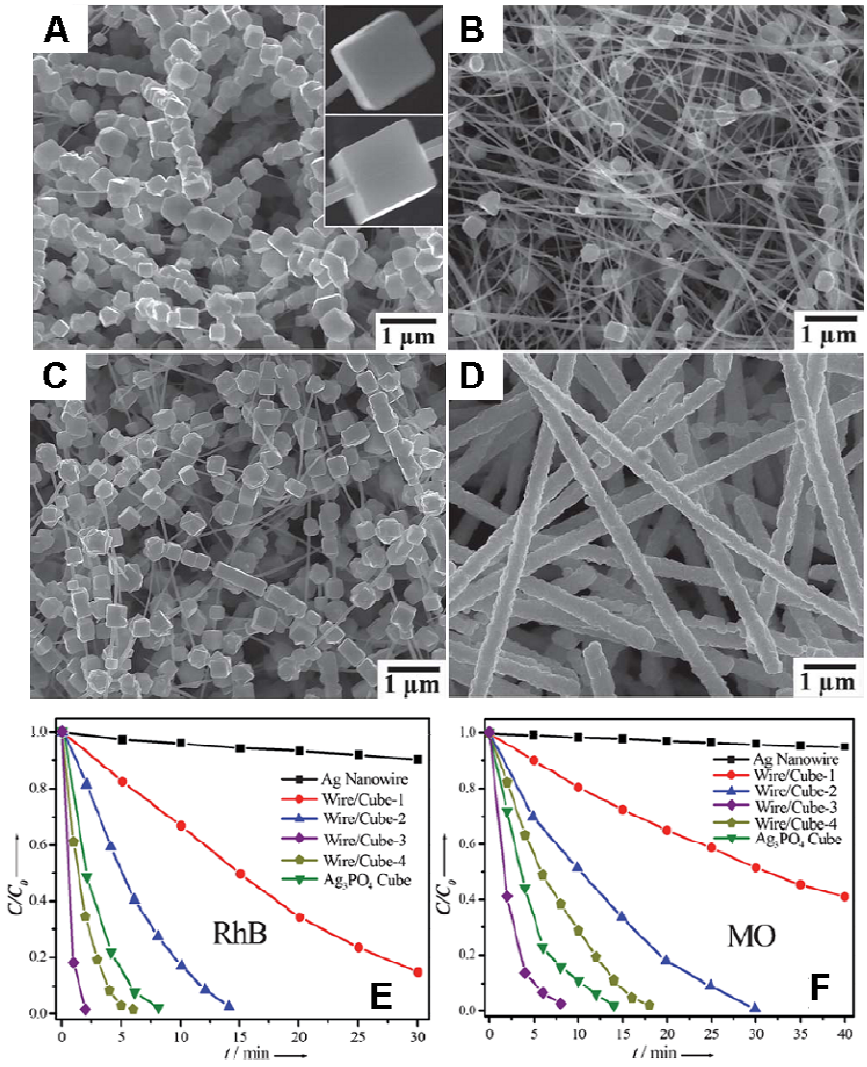

Fig. 4 (A) SEM image of the Ag nanowire/Ag_3PO_4 cube necklace-like heterostructure. (B, C, D) SEM images of as-prepared Ag/Ag_3PO_4 heterostructures with different morphologies by adjusting the concentration of $[Ag(NH_3)_2]^+$ complex: (B: 0.05 M, C: 0.1 M, D: 0.2 M), (E, F) Photocatalytic activities of Ag nanowire/Ag_3PO_4 cube necklacelike heterostructures, Ag nanowires, and pure Ag_3PO_4 cubes for RhB and MO degradation under visible-light irradiation ($\lambda > 420$ nm) (wire/cube-1: sample B; wire/cube-2: sample C; wire/cube-3: sample A; wire/cube-4: sample D) (from ref. 56).

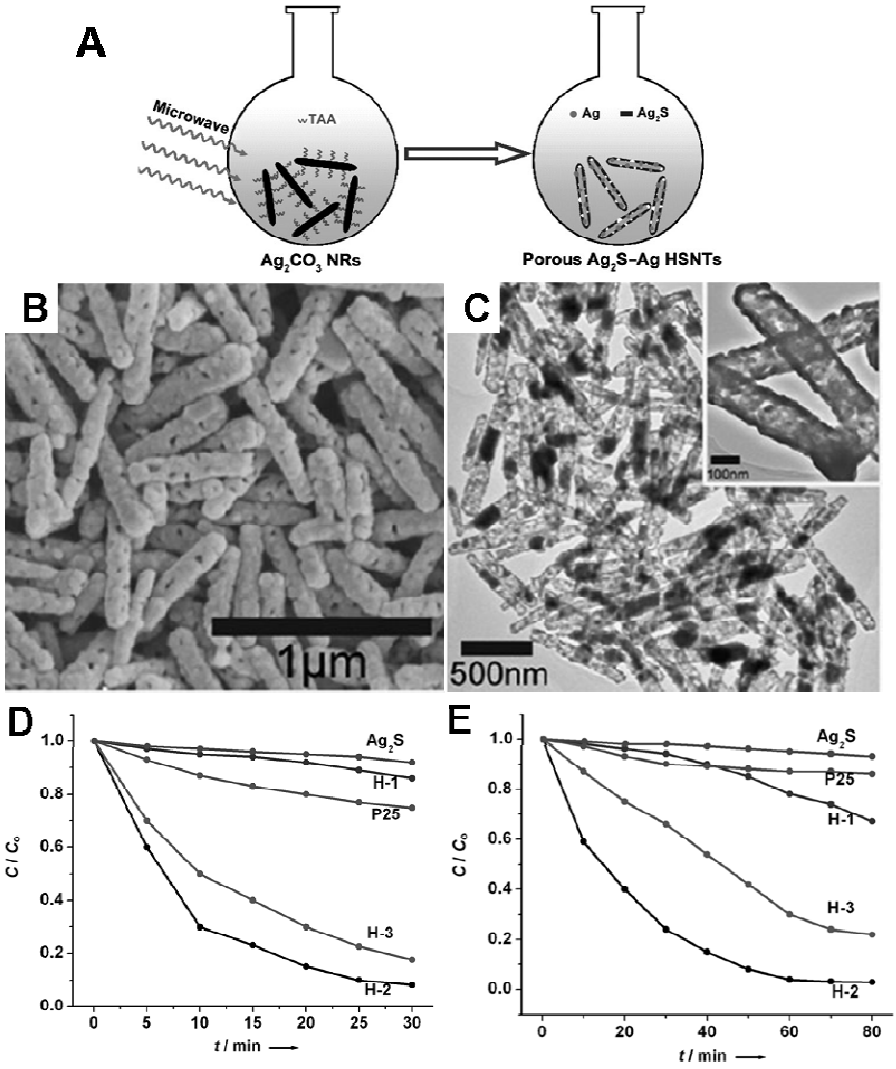

Fig. 5 (A) Illustration of the fabrication of porous Ag_2S-Ag heterostructure nanotubes by a one-pot microwave-assisted method. (B) SEM images of the as-prepared porous Ag_2S-Ag heterostructure nanotubes; (C) TEM images of porous Ag_2S-Ag heterostructure nanotubes (inset: a high-magnification image). (D) Photocatalytic degradation of MO, and (E) photocatalytic reduction of Cr^{VI} in the presence of different photocatalysts. C is the concentration of MO after light irradiation for a certain period, and C_o is the concentration of the MO after reaching adsorption/desorption equilibrium in dark (from ref. 20).

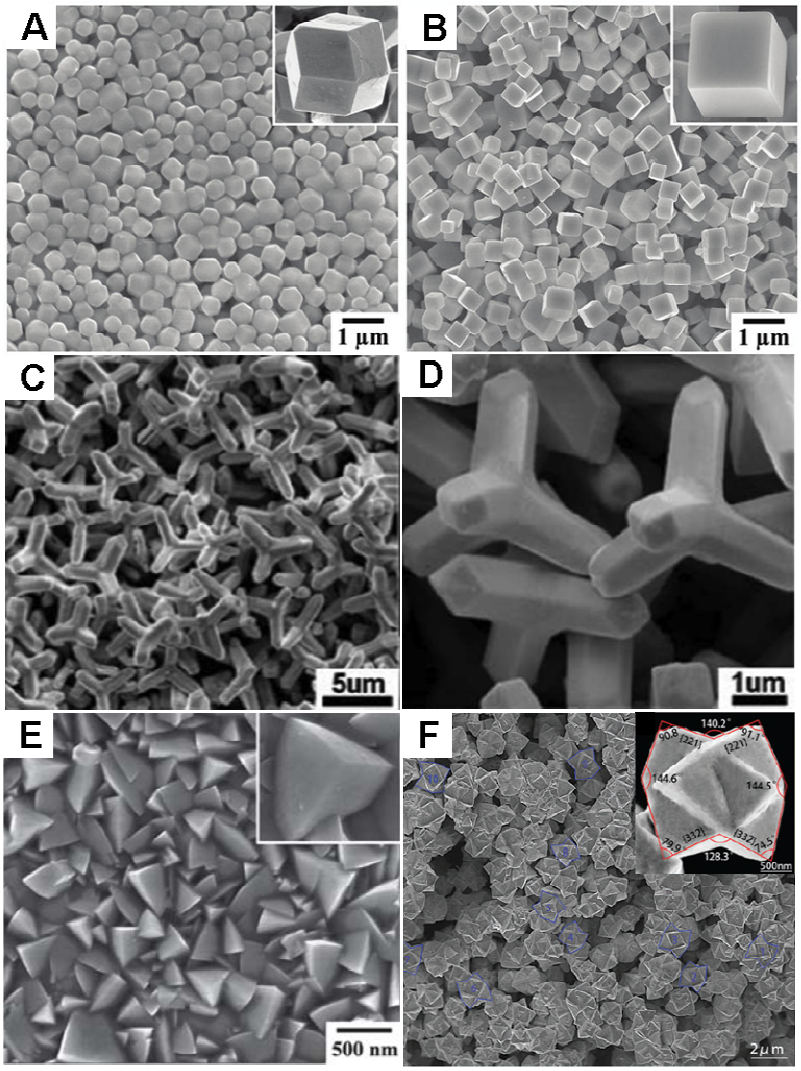

Fig. 6 SEM images of Ag_3PO_4 sub-microcrystals with different morphologies: (A) rhombic dodecahedron, (B) cube (from ref. 66); (C, D) tetrapod at low and high magnifications (from ref. 67); (E) tetrahedron (from ref. 69); (F) trisoctahedron (from ref. 70).

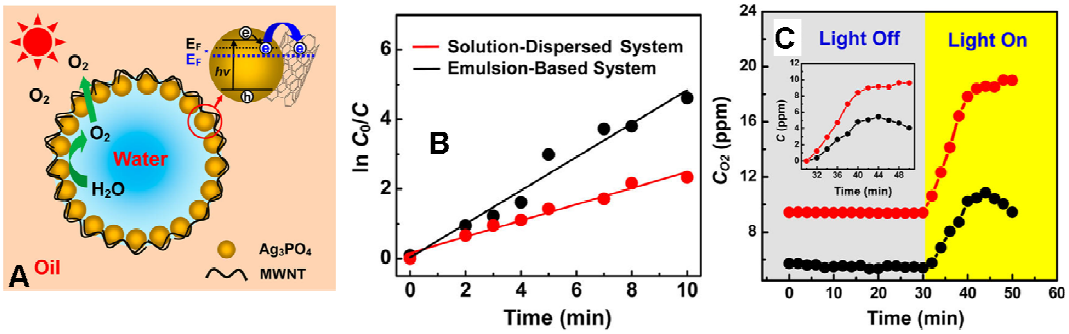

Fig. 7 (A) Schematic of the Pickering Emulsion-based photocatalytic system formed by self-assembling Ag_3PO_4-MWNT nanohybrid at the water/oil Interface. (B) First-order linear transforms of MB decomposition in Pickering emulsion-based system (black) and solution-dispersed system (red). (C) O_2 evolution under illumination in solution-dispersed system and Pickering emulsion-based system. Inset: O_2 yield in the solution-dispersed system (black curve) and Pickering emulsion-based system (red curve) (from ref. 101).

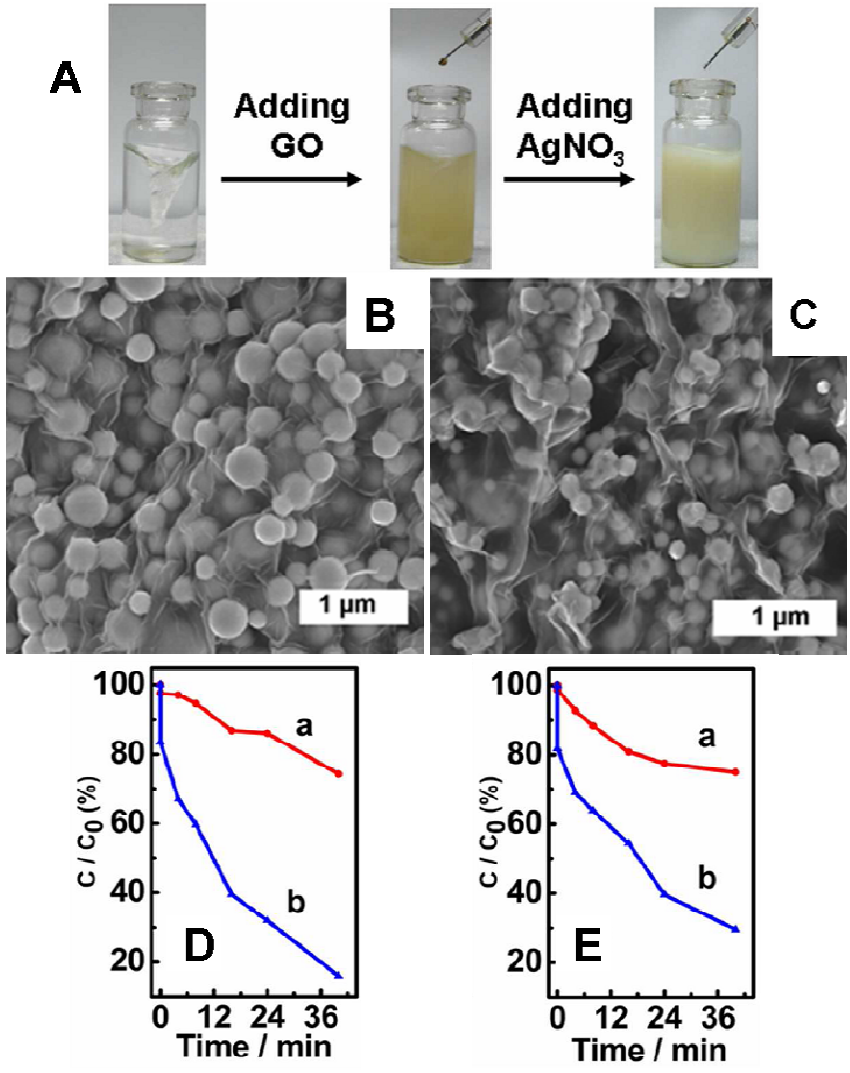

Fig. 8 (A) Illustration of the the preparation of Ag/AgX/GO hybrid nanocomposites via an oil/water system at room temperature. (B, C) SEM images of the synthesized Ag/AgBr/GO and Ag/AgCl/GO, respectively. (D, E) Photocatalytic photodegradation of MO molecules under visible light irradiation (D: AgBr (a) and Ag/AgBr/GO (b); E: Ag/AgCl (a) and Ag/AgCl/GO (b) nanospecies) (from ref. 104).

Table of Content

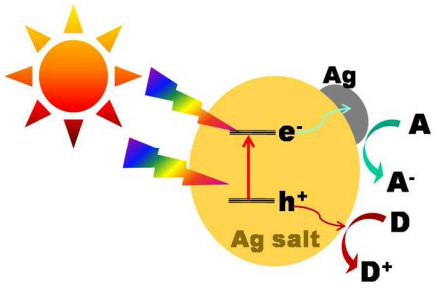

This review summarizes the recent progress in Ag-compound based semiconductor photocatalysts, which will provide insights for future photocatalyst design.